12th AIAA/CEAS Aeroacoustics Conference (27th AIAA Aeroacoustics Conference)
8-10 May 2006, Cambridge, Massachusetts

AIAA 2006-2525

Optimization of Traditional and Blown Liners for a Silent Aircraft

Thomas R. Law* and Ann P. Dowling†
Cambridge University Engineering Department, Trumpington Street, Cambridge, CB2 1PZ, UK

The current form of the Silent Aircraft is a blended wing design with the propulsion system embedded in the rear of the airframe and the intakes located on the upper surface of the wing. Such a design allows for a substantial amount of acoustic treatment in the exhaust duct. Conventional aeroengine liners have the ability to absorb certain modal disturbances very effectively, whilst others can propagate down the exhaust duct virtually unattenuated. On reaching the duct termination, these 'problem' modes will often radiate in a similar direction meaning that the resulting engine noise signature will exhibit a characteristic peak in the rearward arc. Thus, the key to the realization of 'silence' whilst maintaining acceptable engine performance will be based around the ability to eliminate the energy in these acoustic modes effectively. This paper explores the potential for exploiting the different attenuation mechanisms of conventional acoustic and blown liners against the fan rearward broadband noise. To accomplish this, we develop a more intelligent 'cost function' based on radiation patterns as an extension to merely considering integrated levels of residual acoustic power. The numerical optimization of liner parameters for both types is then undertaken by developing and solving appropriate eigenvalue problems based on in-house routines. We find that reductions in acoustic power do not necessarily translate into reductions in peak sound pressure at the observer location. Multiple optimized segments of traditional aeroengine liners were found to be the most effective way of reducing peak observer noise. Although blown liners were very effective at reducing low frequency noise, after A-weighting the overall benefit of a blown liner segment was small.

I. Introduction

THE Silent Aircraft Initiative (SAI) seeks to generate a credible commercial aircraft that would be virtually inaudible outside of a typical 'aircraft boundary'. The current form of the aircraft design is a blended wing body with the propulsion system embedded in the rear of the airframe and the intakes located on the upper surface of the wing (see Fig. 1). Such a design allows for a substantial amount of acoustic treatment in the cylindrical exhaust ducts of the powerplant, although conventional engine noise prediction routines are ill-suited to this kind of geometry. The inevitable installation of a high bypass ratio turbofan engine means that one of the major obstacles to success is the rearward propagating fan noise.

Conventional aeroengine liners have the ability to absorb certain modal disturbances very effectively, whilst others can propagate down the exhaust duct virtually unattenuated. If one considers the acoustic field in terms of ducted ray theory, attenuation is strongly linked to the number of reflections experienced. From the definition of ray angles (see for example, Chapman[1]), the field can be envisaged in terms of caustic cylinders formed by coincident ray paths. Non-spinning modes will propagate through the centre spanning the entire diameter between reflections (i.e. tangential to an infinitely small caustic cylinder). In particular, the plane wave propagates straight down the channel. Higher order modes are contained within increasingly smaller annuli adjacent to the internal surface as cut-off is approached. The net result is that modal attenuation distributions following the introduction of a lined surface will often demonstrate 'modal triangles'. That is, energy dissipation increases rapidly with increasing azimuthal and radial order. A typical fan rearward noise signature for a turbofan engine is shown in Fig. 2. The persistent feature is the peak in the rearward arc at around 45 degrees from the exhaust axis. In order to meet the SAI noise target, we must eradicate this peak but first it is essential that we understand how it is formed. Chapman[1] also applied ray theory considerations to the diffracted field at the duct termination by extending the Geometrical Theory of

* Research student, Department of Engineering, trl27@cam.ac.uk
† Professor, Department of Engineering, AIAA Member.

Diffraction[2] (normally associated with optics). In the presence of uniform flow, a ray that impinges on the duct lip forms a conical surface of diffracted rays. This is obtained by extending the incident wave past the point of impingement and rotating about a tangent to the rim. It is shown that the maximum irradiated angular range does not depend on the radial order of the propagating mode. Given that there are infinitely many rays striking the edge of the duct, the rotational symmetry defines a cone of silence for each mode. Under these conditions, the only modes that can radiate along the direction of the exhaust axis are the non-spinning ones (no cone of silence). Increasing the azimuthal order at a fixed frequency results in an enlargement of this cone of silence, where the modes closest to cut-off will radiate principally at ninety degrees to the exhaust direction.

In close proximity to an airport, the assumption of a universal uniform flow is a poor one. The velocity mismatch between the exhaust jet and the ambient flow coupled with the variation in sound speed causes the emitted rays to be refracted away from the exhaust axis. Thus, the radiation produced by low order azimuthal modes that would have radiated close to the exhaust axis will now be refracted to form the peak in the noise signature. These observations are consistent with results computed from the exact solution derived using the Wiener-Hopf technique. Many authors have produced analytical solutions of varying complexity to model turbofan radiation. The most general solution to date is that of Munt[3] who considered the problem of sound propagating through a jet issuing from a circular pipe and studied the effect of various parameters on far-field directivity. Gabard and Astley[4] have extended the Munt solution by incorporating an infinite centre body to model the radiation from a three-quarter cowl engine more accurately. The effect of translating the peak in the noise signature from the exhaust axis is shown explicitly in their paper by varying the velocity mismatch across the vortex sheet. Neither model manages to curtail the exponential growth of the Kelvin-Helmholtz instability in the shear layer to allow it to be represented in the farfield. Consequently the contribution is omitted, yet agreement with experimental data is generally very good and a large proportion of the sound close to the exhaust axis now appears to originate from rays reflected along the cylindrical channel created by the vortex sheet. It seems clear that the key to reducing the peak in the noise distribution lies in removing modes of low azimuthal order more effectively than has been achieved in the past.

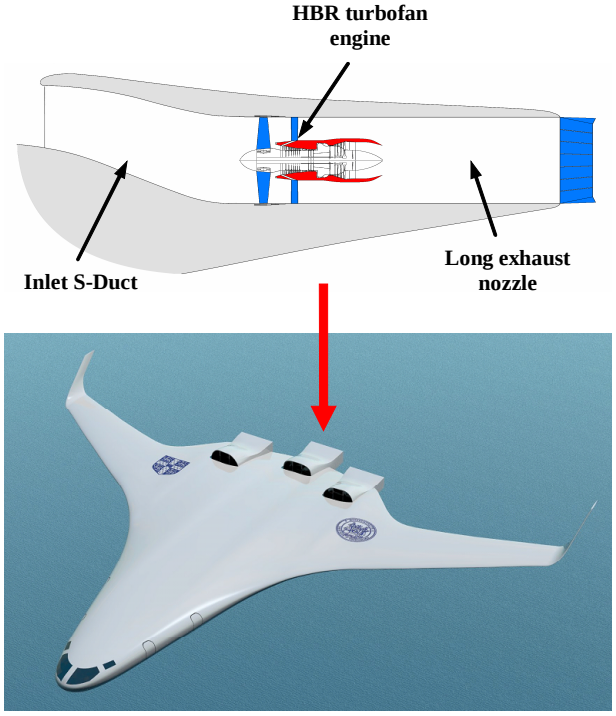

Figure 1. The Silent Aircraft eXperimental (SAX) 20 embedded engine configuration.

The application of perforated liner treatment is not purely restricted to that of noise control. The conditions under which gas turbines and jet engines operate often encourage the formation of combustion instabilities. The installation of a passive damping device can be used to suppress these instabilities by dampening the acoustically-driven disturbances. Bias flows in liners were originally introduced into modern combustion systems as a method of cooling the surface material to ensure satisfactory operation. However, the introduction of a secondary flow has produced some remarkable results on the ability of the liner

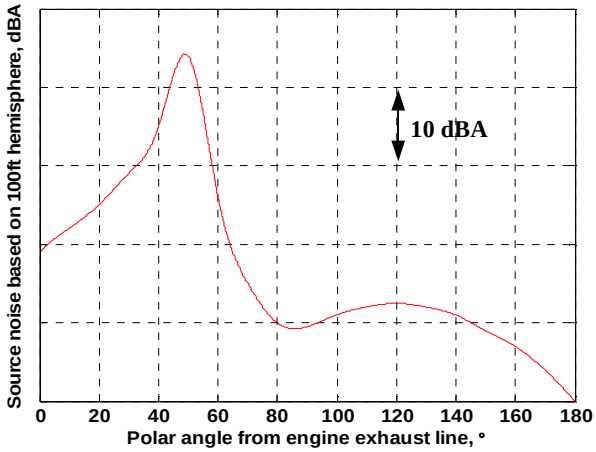

Figure 2. Typical fan rearward noise signature based on empirical data.

to absorb sound. Eldredge and Dowling[5] have shown that, for a duct termination that encourages most of the acoustic energy to be reflected upstream towards the source, as much as 83% of the plane wave energy can be absorbed. Whereas traditional liners utilize a porous facing sheet to encourage vortex shedding and viscous dissipation, blown liners exploit an additional mechanism for the conversion of acoustic energy into vortical fluctuations at the rims of the liner apertures: the incident acoustic waves modulate the bias flow through the apertures enhancing the unsteady vortex shedding and the exchange of energy between acoustic and vortical disturbances. The possibility of non-conservation of acoustic energy in a flow containing vorticity was demonstrated by Morfey[6]. This mechanism has since been shown to occur for many geometries, see for example, Bechert[7] and Howe[8]. Howe[9] also presented an analytical model for the Rayleigh conductivity of an aperture with a bias flow, which he extended to the case of an infinite screen. Despite the considerable benefits observed in combustion systems, any application to acoustic liners is well within its infancy. Hughes and Dowling[10] investigated an infinitely backed screen theoretically and experimentally with a view to suppressing jet 'screech' and 'buzz'. They found that absorption was greatest if the incident acoustic wave was capable of exciting a Helmholtz-type resonance in the cavity. Zhao and Sun[11] explored the active tuning of both cavity depth and bias flow to achieve a specified wall impedance and maximum absorption. The importance of liner thickness, assumed negligible in these previous analyses, was confirmed experimentally by Jing and Sun[12]. Further research has been carried out by Eldredge[13] on how such a system interacts with the higher order modes. His approach is to model the liners with effective compliances, employing a Green's function methodology to decouple the duct from the surrounding cavities, and solve for the fluctuating pressure distribution. The results have been validated by experiment and show good absorption for low order modes, particularly at lower frequencies.

In the present paper, we explore the scope for optimization of traditional liners in conjunction with blown ones to achieve the maximum perceived noise reduction for an observer on the ground. In Section II, we develop a more intelligent 'cost function' based on far-field modal radiation patterns as an extension to merely considering integrated levels of residual acoustic power. We then go on to observe the benefits of targeting particular modes using different liner models: traditional (Section III) and blown (Section IV). Both systems are numerically optimized for the SAI exhaust by solving appropriate eigenvalue problems using in-house routines. The latter is an extension of the model created by Eldredge[13]. Section IV concludes by briefly exploring the potential attenuation benefits available for a combination of both liner types to the SAI design.

II. Development of an Appropriate Cost Function

Before we begin any detailed consideration of liner modeling, it is instructive to consider the metric against which a liner should be optimized in light of the comments made in the previous section. In this section, we present two different metrics for comparing liner effectiveness. Both will be used in due course as a means of demonstrating the importance of modal directivity on liner performance. The first is a simple consideration of acoustic power whereas in the second, we develop a metric that targets disturbances that affect the observer more directly.

A. Residual Acoustic Power at the Nozzle Exit

An intuitive place to begin when looking for a metric to compare liner designs is to minimize the acoustic energy flux that reaches the end of the nozzle. Firstly, we consider a time harmonic pressure field with an exp(iωt) dependence in a uniform mean flow in a duct of radius a. Within the duct, co-ordinate system *(r, θ, x)*, the acoustic pressure field, *p*, associated with modes traveling downstream can be expressed by the following modal expansion:

$$p = \sum_{n=-\infty}^{\infty} \sum_{m=1}^{\infty} A_{nm} \exp(i\omega t - in\theta - ik_x^{nm} x) J_n(k_r^{nm} r) \tag{1}$$

Here, *n* and *m* are the azimuthal and radial mode orders, k_x and k_r represent wavenumbers in the axial and radial directions, A_{nm} is an amplitude coefficient and J_n denotes the nth order Bessel function of the first kind. In a uniform axial mean flow, Eq. (1) satisfies the convected wave equation if the axial and radial wavenumbers are related by:

$$k_x^{nm} = \frac{-kM_j + \sqrt{k^2 - (1 - M_j^2)(k_r^{nm})^2}}{1 - M_j^2} \tag{2}$$

M_j is the mean flow Mach number, U_j/c_j, and k is the free-space wavenumber, ω/c_j. The speed of sound, c_j, is assumed constant in the duct. The power transmitted downstream is obtained by evaluating a generalized expression of acoustic intensity (see Appendix A) and summing over the cut-on modes. Clearly, the amplitude of the waves will vary with axial position as the duct wall has a finite acoustic impedance associated with it. If the modal coefficients, A_{nm}, are set at a given axial position, x_0, we can express the residual power as a function of x by incorporating the decay rate (Eq. (3)).

$$P(x) = \frac{\pi}{\rho_j c_j} \sum_{n=-n_{\max}}^{n_{\max}} \sum_{m=1}^{m_{\max}^n} |A_{nm}|^2 \exp\left[2\,\mathrm{Im}(k_x^{nm}(x-x_0))\right] \times \left[\left(1+M_j^2\right)\mathrm{Re}(\eta_{nm}) + M_j\left(1+|\eta_{nm}|^2\right)\right] \int_0^a \left|J_n(k_r^{nm} r)\right|^2 r\,dr \qquad x \geq x_0 \tag{3}$$

$$\eta_{nm} = \frac{k_x^{nm} a}{\left(ka - M_j k_x^{nm} a\right)} \tag{4}$$

In practice, we will use a variation of Eq. (3) to set modal amplitudes at the start of the liner and compute attenuations that determine the residual acoustic power at the exit (see Sections III and IV). However, for optimization purposes we require a scalar measure of liner performance. For this, we will compute an attenuation sound power level (PWL) at each of the third-octave centre frequencies from 50Hz to 10kHz. This can be subtracted from the power levels produced by the source to give residual sound power levels. An appropriate metric can then be formed by integrating the mean-squared pressure over the frequencies whilst applying an A-weighting.

B. Peak Sound Pressure at Ground Level

The metric presented in Part A will treat the A-weighted energy flux in each propagating mode equally. We now move on to develop a more comprehensive metric that encapsulates much of the discussion in Section I. Consider the diagram below showing an aeroengine exhaust nozzle elevated above the ground. We will look to minimize the peak sound pressure on the horizontal line, Ω, H meters below the aircraft in the same frame of reference. At this stage, we will ignore any effects due to lateral attenuation and atmospheric absorption.

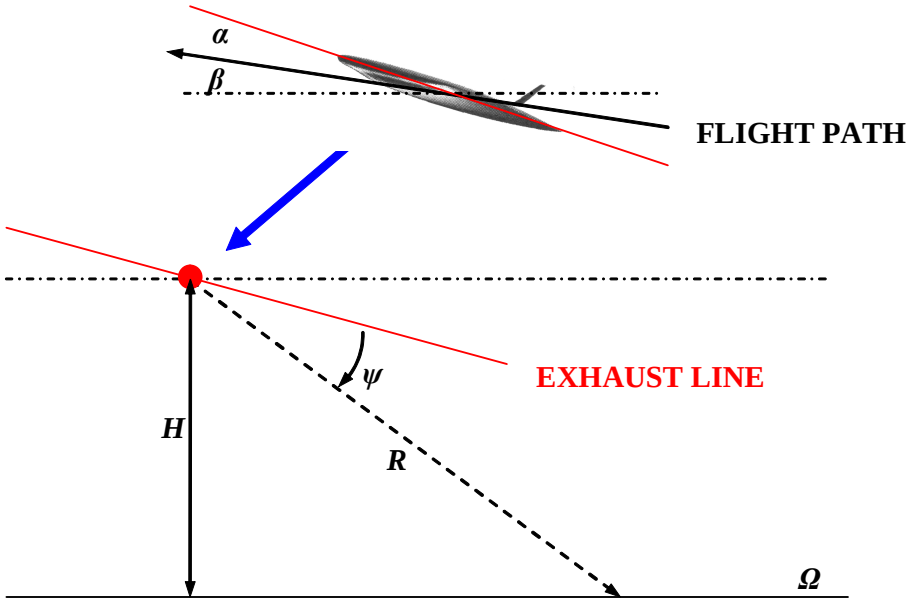

Figure 3. Schematic showing the system used to derive a more intelligent cost function.

The nozzle is tilted in line with the incidence angle of the aircraft. The angle between the exhaust line and the horizontal plane being equal to the angle of attack, α, plus the aircraft climb angle, β. Hence, the distance, R, that a ray emitted from the source will have to travel before it impinges on Ω will be given by the relationship $H/\sin(\psi + \alpha + \beta)$. The inclination of the exhaust line relative to the ground is significant as it can have a large effect on the distance an acoustic ray will have to travel. This can be formally cast into a suitable design metric. The radiated pressure field can be defined in spherical co-ordinates (R, θ, ψ) using a similar expression to that of Gabard and Astley[4] (see Eqs. (5) and (6)). The term $D_{nm}(\psi)$ is a modal directivity factor whilst the function $S(\psi)$ accounts for the wavefront stretching due to the ambient flow. B_{nm} is an equivalent coefficient to A_{nm} in Eq. (1) that corresponds to acoustic energy transmitted from the nozzle and M_0 is the free stream Mach number.

$$p_{nm}(\psi, R) = \frac{|B_{nm}| D_{nm}(\psi)}{R} \exp\left(-\frac{i\omega R}{c_0} S(\psi) + i(n+1)\pi/2\right) \tag{5}$$

$$S(\psi) = \frac{\left(1 - M_0^2 \sin^2\psi\right)^{1/2} - M_0 \cos\psi}{1 - M_0^2} \tag{6}$$

We can compute good estimates of $D_{nm}(\psi)$ numerically using the Wiener-Hopf solution due to Munt[3]. If we can determine the amplitude of each cut-on mode immediately following its exit from the duct, the sound pressure level on the line (assuming no correlation between modes) as a function of polar angle is given by:

$$SPL(\psi) = 10\log_{10}\left[\sum_{n=-n_{\max}}^{\eta_{\max}} \sum_{m=1}^{m_{\max}^n} \left|\frac{B_{nm} D_{nm}(\psi)}{\sqrt{2}\, p_{ref}}\right|^2 \left[\frac{\sin(\psi + \alpha + \beta)}{H}\right]^2\right] \qquad \begin{matrix} 0 < \psi + \alpha + \beta < \pi \\ kH >> 1 \end{matrix} \tag{7}$$

To address the broadband nature of the source noise, sound pressures can be evaluated at each of the third-octave centre frequencies and integrated in a similar fashion to the residual acoustic power metric. However, the scalar value monitored here will be the peak dBA value on the horizontal surface representing the ground. Within the metric, we also account for ground reflection effects from a rigid surface by incorporating an enhancement of 3dB at each centre frequency. This is in line with recommendations made by Pierce[14]. It is worth highlighting the fact that in this model the pitch angle of the aircraft causes some of the rays emanating from the hemisphere below the aircraft not to reach the ground and hence the corresponding directivity factors are essentially unused.

III. A Conventional Liner Optimization Model

First, we will examine the modal attenuation characteristics associated with a conventional liner by considering a simplified eigenvalue problem.

A. Model Background

The model developed to estimate the attenuation for a conventional lined duct is similar in principle to that given by Ko[15]. The acoustic field within the duct satisfies the convected wave equation. If we assume a purely inviscid uniform axial flow in conjunction with an anechoic exit condition downstream, the pressure field can be expressed using a similar modal expansion to Eq. (1). The modes in the lined duct can be found by matching the acoustic waves to the liner impedance. The fluid displacement at the surface, $r = a$, must match that of the liner. With the existence of a mean flow, the fluid normal velocity must equal the material derivative of the surface displacement, ε.

$$u_{r=a} = \left[i\omega + U_j \frac{\partial}{\partial x}\right]\varepsilon \tag{8}$$

The normal velocity of the wall and the normalized acoustic impedance, Z, can be used to eliminate the surface displacement. With a little algebraic manipulation, we arrive at the local boundary condition in terms of the acoustic pressure.

$$\left.\frac{\partial p}{\partial r}\right|_{r=a} = -\frac{i\omega}{Zc_j}\left[1-\frac{iU_j}{\omega}\frac{\partial}{\partial x}\right]^2 p_{r=a} \tag{9}$$

Insertion of Eq. (1), allows the transformation of this condition into a simple eigenequation where the eigenvalues characterize the effectiveness of the lined surface.

$$k_r^{nm} a \frac{J_{n+1}(k_r^{nm} a)}{J_n(k_r^{nm} a)} - n - \frac{ika}{Z}\left[1-\frac{k_x^{nm}}{k}M_j\right]^2 = 0 \tag{10}$$

B. Solution Scheme and Optimization Framework

A numerical Newton-Raphson scheme is used to converge to the required eigenvalues for all of the cut-on modes at the desired frequency. A correct solution is ensured in each case by tracking the root from the rigid wall case on the real axis. The impedance boundary condition is derived from liner parameters based on either a single or double layer system to ensure a physically realizable result[16, 17]. Acoustic liners contain a number of different parameters that affect resistance and reactance values. For perforate liners, the key parameters are the cell depths and sheet porosities (open-area ratio). These determine both the resonant frequency and the damping of the incident wave. Other parameters such as sheet thickness and perforate hole diameter are required to be as small as possible for optimal performance and therefore the limits tend to be based around material and manufacturing constraints. For this reason, we will use parameter values typical of liners currently in service.

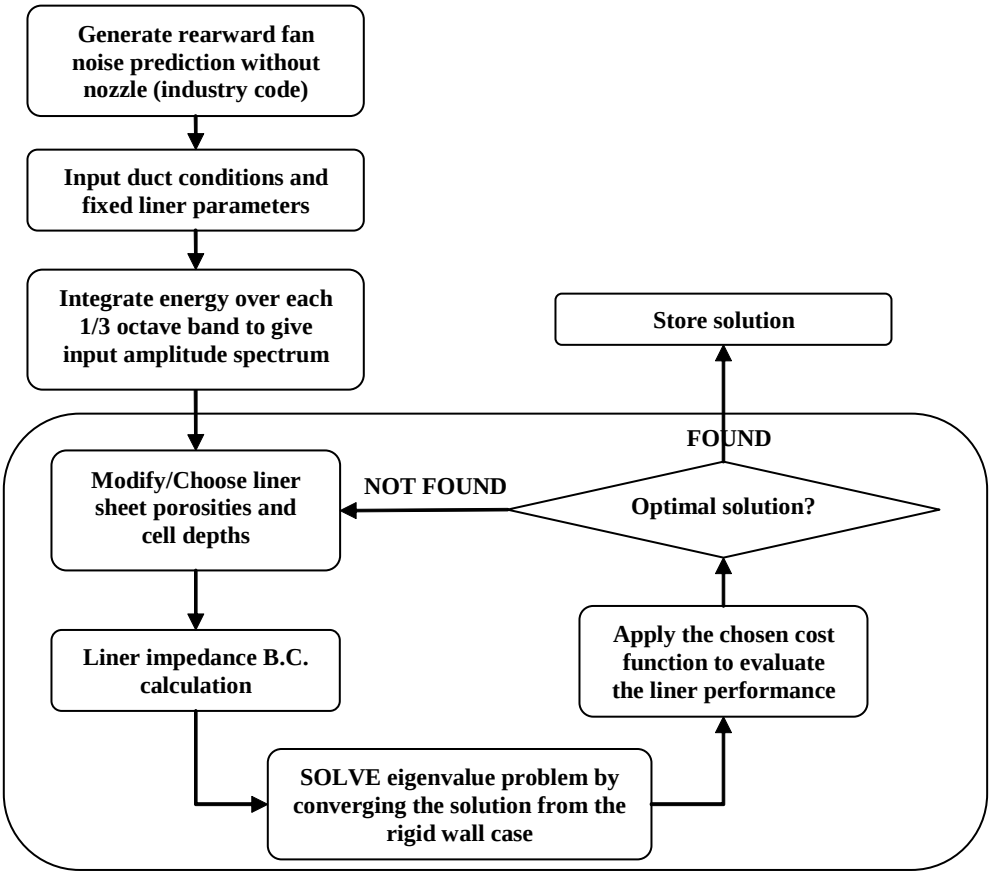

Figure 4. Optimization routine for a conventional liner - single or double layer.

The optimization routine is outlined in the flowchart of Fig. 4. The fan source noise (against which to optimize the liner) is supplied by an industrial engine noise software package. This includes attenuation due to the presence of bypass liners, allowing the energy at a given frequency and hence the appropriate modal amplitudes to be applied to each mode at the start of the duct. To simulate broadband noise, we make the usual assumption of equal energy per mode and allocate amplitudes at the start of the lined section using the rigid wall condition derived in Appendix A. This assumption is valid due to the fact that no energy dissipation will have occurred before this point and it will ensure that liner performance can be compared objectively without fear of any bias from an evolving equal energy assumption. Evaluating modal amplitudes outside of the main optimization loop is also beneficial to the overall runtime of the algorithm. The relevant expression is given in Eq. (11).

$$P_{nm} = \frac{\pi a^2 |A_{nm}|^2}{2\rho_j c_j}\left[\left(1+M_j^2\right)\eta_{nm} + M_j\left(1+\eta_{nm}^2\right)\right]\left[J_n^2(k_r^{nm}a) - J_{n-1}(k_r^{nm}a)J_{n+1}(k_r^{nm}a)\right] \quad (11)$$

The routine is based around the multi-dimensional optimization tools within Matlab. The model has been formulated so that the only variables changed within the optimization are the cell depths and porosities. That is, two variables in the case of a single layer liner and four when optimizing two layers. The two cost functions presented in the previous section have been applied separately to allow comparisons to be drawn with the resulting liner designs.

C. Single/Double Layer Optimization Results

The current design of the Silent Aircraft allows for a maximum exhaust nozzle length-to-diameter ratio of two based on a fan diameter of 1.29m. We choose to optimize a conventional liner for a single exhaust nozzle at the position of maximum engine noise during the take-off trajectory[18]. The relevant parameters for the peak observer noise cost function at this point are given in Table 1, alongside the A-Weighted PWL and peak SPL values before the effects of the nozzle are applied. Results are presented for both uniform single and double layer liners using both cost functions. In addition, the values of both cost functions have been included for the final designs to facilitate comparison.

Table 1. Parameters used in cost functions

Parameter	Value
Angle of attack, °	**8.84**
Climb angle, °	**6.61**
Aircraft height, m	**76.0**
Residual PWL without nozzle, dBA	**129.7**
Peak observer SPL without nozzle, dBA	**87.02**

The results summary shown in Table 2 presents a general indication of what has been achieved, however it is more instructive to view a mode-by-mode breakdown of energy absorption. As liner performance varies substantially with frequency, it is insufficient to compare results at constant frequency. A more suitable comparison can be made if we integrate the attenuated energy over each frequency whilst applying an A-weighting. Since the majority of the high order modes are cut-off at low frequency, the modal absorption triangles that normally form (see Fig. 5) will be lost. However, this is a much fairer means of comparison but one should only consider relative changes in the bar heights between liners and not absolute values.

The routines have converged to liner parameters that do not look out of place compared to existing acoustic treatments. As expected, the double layer liner is more effective than the single one. This is no surprise as the range of impedances is drastically increased by the extra degree of freedom. The main result to note is the discrepancy between residual

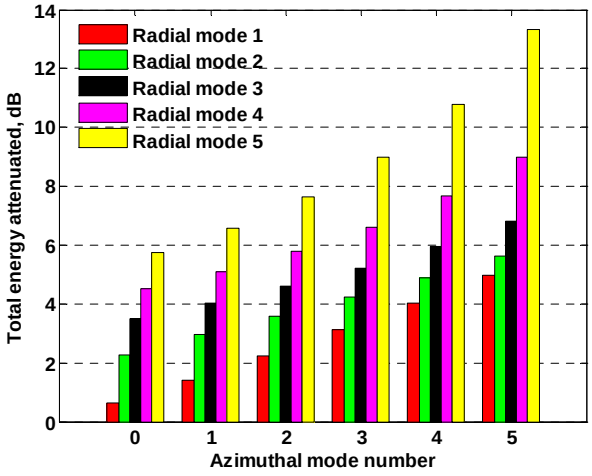

Figure 5. Low order modal attenuation at 2000Hz, optimized double layer liner, cost function A.

Table 2. Results for optimized single and double layer liners.

	Single layer liner		Double layer liner	
	Cost function A	Cost function B	Cost function A	Cost function B
Upper cell depth, mm	40.40	75.11	62.18	152.02
Facing sheet porosity, %	10.23	5.56	14.21	79.54
Septum cell depth, mm	N/A	N/A	97.19	7.00
Septum porosity, %	N/A	N/A	11.43	5.63
PWL at nozzle exit, dBA	119.1	120.8	117.2	119.5
Peak observer SPL, dBA	82.41	81.32	82.86	80.75

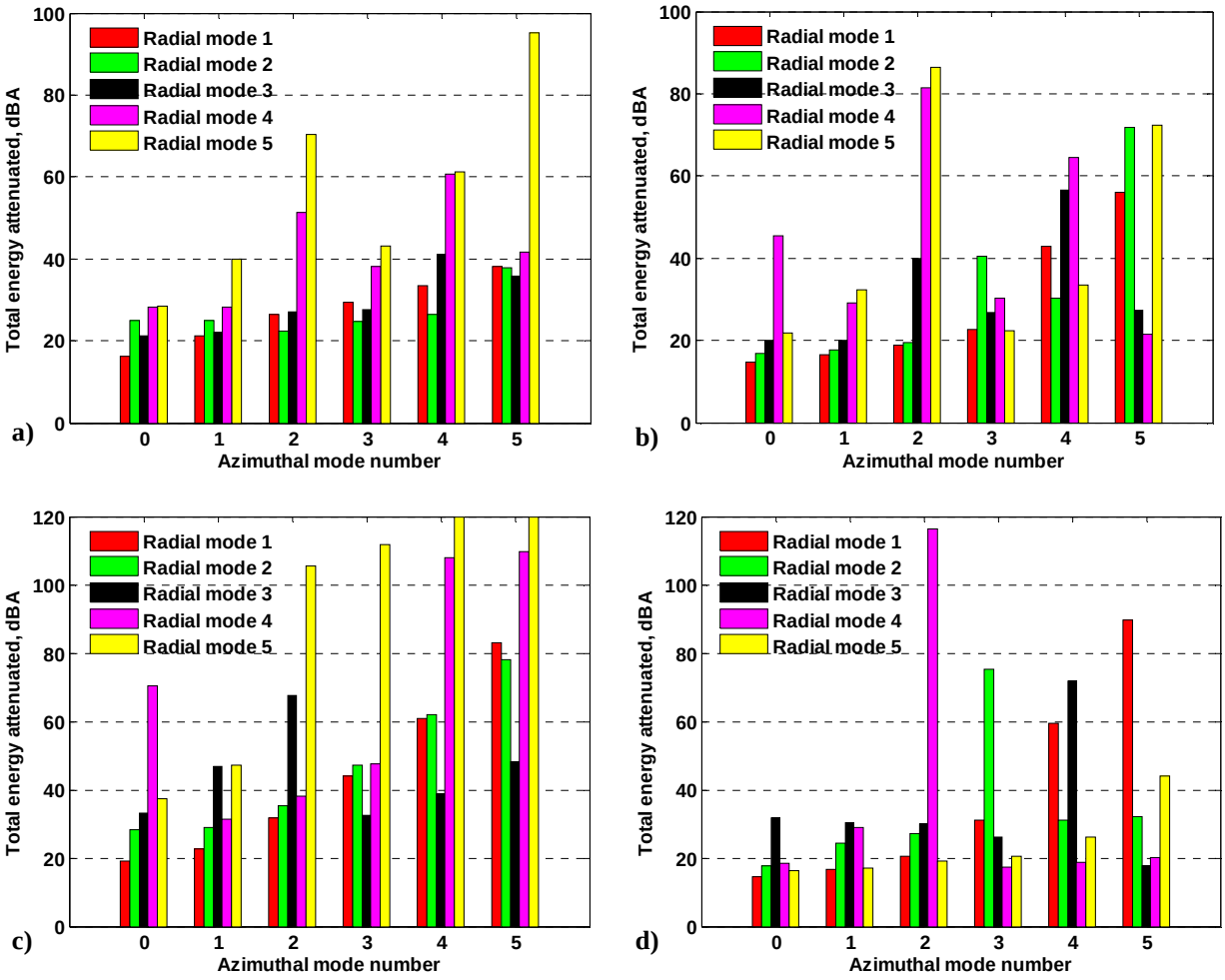

Figure 6. Integrated modal attenuation plots for optimized liners. Single layer (a, b) using cost functions A, B and double layer (c, d) using cost functions A, B respectively.

acoustic power and peak observer sound pressure. A decrease in one of the metrics does not guarantee a corresponding decrease in the other. This effect is more notable for double layer liners as might be expected.

The data in the attenuation plots are more difficult to interpret. We know that the low order modes in their unattenuated state are the most effective radiators and therefore, one might expect to observe a distinct increase in the attenuation of these modes when using the second cost function. On further reflection, the situation is more complicated than this. During optimization as the routine seeks to 'attack' the modes that contribute most effectively to the noise peak, the peak will be diminished meaning that other modes will become more prominent. Attention will then be diverted to these modes until they are no longer the most important. If the routine seeks to purely reduce acoustic power, attenuation will be obtained from the easiest possible location. A general look at the results for individual frequencies reveals that the attenuation spectra from cost function A tend to be punctuated by large spikes where the modes are easiest to absorb. In contrast, cost function B will produce a more uniform attenuation distribution. The fact that the double layer liner has produced lower levels using cost function B (Fig. 6(d)) than the single one (Fig. 6(b)) suggests that the additional modal attenuation seen in the latter does not significantly affect the observer. Hence with two degrees of freedom, the optimization has chosen to concentrate on energy elsewhere.

Based on these results, it appears there is significant merit in optimizing liners by considering the ensuing farfield radiation patterns.

D. Multiple Liner Estimates

Invariably, the acoustic treatment within an aeroengine exhaust will incorporate a number of different lined segments to address the broadband nature of the source noise more effectively. At this stage, we will gain an estimate for the attenuation achievable by a combination of single layer liners by neglecting any scattering effects due to the impedance changes at the interfaces. It is expected that the results presented here will represent a lower limit of what can be achieved as we are not taking advantage of either double layer liners or preferential scattering. A more refined model to incorporate these effects will be developed in due course, however this model will be useful as a first approximation as it allows us to select from a wider range of liners to find the most effective. This is primarily because the optimization of each segment is decoupled from the others meaning that the order in which the liners are placed also becomes irrelevant. In addition, it is thought that scattering may be less important for a longer exhaust such as that of SAX 20. We have already seen that the modes closest to cut-off are readily absorbed and these are the ones that are most susceptible to scattering. Furthermore, the rotational symmetry of the problem ensures that scattering will not take place between azimuthal orders and as the peaks in the radiation patterns are a strong function of n values, the effect might not be as pronounced as initially thought.

Under these assumptions, we can estimate the amplitude squared pressure of each downstream propagating mode by accounting for the axial decay rates due to the presence of q_{max} different liners (Eq. (12)).

$$\left|B_{nm}\right|^2 = \left|A_{nm}\right|^2 \prod_{q=1}^{q_{\max}} \exp\left[\frac{4L_q}{D}\,\mathrm{Im}(k_{x_q}^{nm} a)\right] \tag{12}$$

Having multiple lined segments in the exhaust raises another question as to how much of each one to install to obtain the most effective reduction in the source noise. This has been dealt with by implementing the following procedure:

1. Choose a selection of cell depths (essentially a selection of possible liners).
2. Run the optimization loop outlined in Fig. 4 to obtain the eigenvalues for a unit L/D of each liner.
3. Express the metric as a simple function of liner *L/D* ratios based on Eq. (12).
4. Run a second optimization loop to find the best combination of lengths against the same cost function.

This algorithm allows unsuitable liners to be disregarded by setting the corresponding *L/D* ratio to zero.

The program was given a choice of 57 cell depths that should perform well at a wide cross-section of frequencies between 50Hz and 10kHz. Results have been obtained for both cost functions but in the interest of brevity, a summary is shown in Table 4 whilst the details of each optimized segment have been included as Appendix B. In addition, the liner length optimizer has been executed multiple times to observe the change in residual power and observer sound pressure as the overall length of the exhaust nozzle is varied. The effect is shown graphically in Fig. 7.

Table 4. Results for optimized multi-specification liners.

	Cost function A	Cost function B
PWL at nozzle exit, dBA	**114.5**	**118.5**
Peak observer SPL, dBA	**81.80**	**79.82**

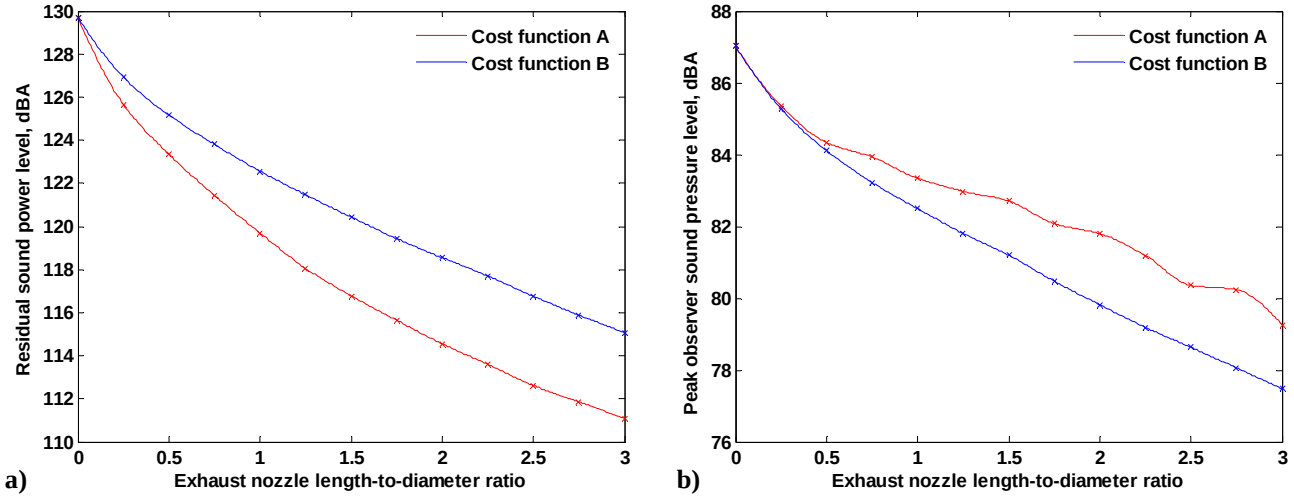

Figure 7. The variation of a) residual sound power level and b) peak observer sound pressure level for optimized multi-specification liners of increasing nozzle length.

The multi-specification liner design has exaggerated the effects observed whilst optimizing the single layer liner by ensuring that the performance is more consistent over the range of frequencies. Comparison of the two metrics in Table 4 provides more support for the remarks made in Part C. Some insight into how the energy is being removed is provided by Fig. 7. For a short nozzle ($L/D < 0.25$), the choice of cost function does not have a marked effect on observer sound pressure. As we move to a more appreciable nozzle length, we begin to see divergence between the two. The rate of A-weighted energy removal exhibits exponential decay in both cases but the rate is slower for B as it targets energy that is more awkward to remove. This has materialized in Fig. 7(b) as a constant decay rate for curve B as the noise peak is eroded. The behavior of curve A is much more erratic with the liners opting to remove energy from modes that do not always contribute significantly to the peak for that particular nozzle length.

IV. Blown Liner Optimization

The tools required to evaluate the performance of a blown liner exist in a rudimentary form as a consequence of earlier research undertaken by Eldredge[5, 13]. The ongoing work with blown liner optimization requires the modification of the small scale low frequency system into something that resembles the mixed exhaust of the Silent Aircraft.

A. Model Background

The finer details of the model can be found here[13] and we will only present a brief summary to inform the reader. The Fortran software computes the attenuation and scattering of an incident acoustic field as it interacts with a series of blown concentric liners downstream. It allows for the evaluation of annular ducts surrounded by an arbitrary number of liners. However, the system that we will study will be the cylindrical single cell system shown in Fig. 8. This contains two perforated sheets to allow the air to pass into the duct. Each perforated sheet contains a uniform series of small apertures as shown. The liners are modeled using effective compliances by distributing the acoustic volume flux over the associated cell of side d_h and including a term for the inertia of the fluid within the liner thickness[9]. This accounts for the absorption generated by the vorticity shed from the rim. The symbols used to identify the upstream and downstream traveling modes are equivalent to the modal coefficients used earlier in this paper only now we include +/- to identify downstream/upstream propagating disturbances.

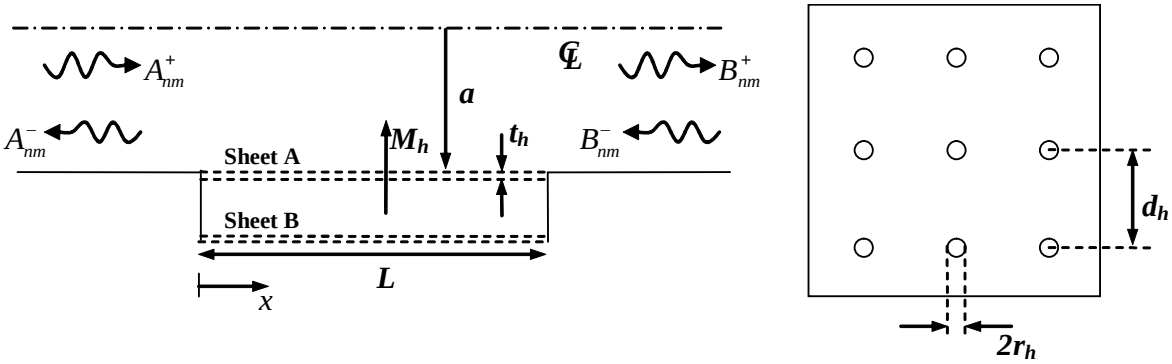

Figure 8. Schematic showing the blown liner model to be optimized for the SAX 20 exhaust nozzle.

The current form of the software does not account for the presence of a mean flow in the duct, although the ongoing work on blown liners will involve the extension to mean flow in due course. The major differences will be the effect that a grazing flow will have on the liner compliance and the inclusion of convected terms in the acoustic intensity (currently only the time-averaged pressure velocity product). Eldredge classified the performance of a liner in terms of an absorption factor defined to be the fraction of acoustic energy that enters the lined section but does not leave it, Eq. (2.34) of Ref. 13. We will alter the definition of absorption slightly as the application is the suppression of rearward propagating fan noise and not combustion instabilities. Energy propagating upstream is considered attenuated as the SAX20 embedded engine installation allows for substantial shielding of forward propagating noise. Hence, it is now defined to be the fraction of acoustic energy that does not exit *downstream* of the lined section. In addition, we are no longer interested in the attenuation of a single incident mode but of all the cut-on modes at a particular frequency. If the unit amplitude of the incident wave assumption is dropped to allow for equal energy and we specify an anechoic end condition to maintain consistency with earlier work; Eldredge's criterion, Δ, is redefined using our nomenclature as:

$$\Delta \equiv 1 - \frac{\sum_{n=-n_{\max}}^{n_{\max}} \sum_{m=1}^{m_{\max}^n} k_x^{nm} \left| B_{nm}^+ \right|^2 \left| J_n(k_r^{nm} r) \right|^2}{\sum_{n=-n_{\max}}^{n_{\max}} \sum_{m=1}^{m_{\max}^n} k_x^{nm} \left| A_{nm}^+ \right|^2 \left| J_n(k_r^{nm} r) \right|^2} \tag{13}$$

The absence of a mean flow will mean that the values computed as part of this investigation will only be initial approximations. However, it will help decide whether such an extension is likely to yield any benefits. Appropriate checks have been carried out (in a similar manner to Eldredge) to confirm that the inherent error caused by truncating the cosine expansion of the Green's function does not lead to an unacceptable loss of accuracy.

B. Optimization Framework

The number of parameters involved in a blown liner system makes generating analytical optimization rules prohibitive. Eldredge attempted to provide a set of criteria for optimal liner design and encountered some difficulty because of this very reason. In the low frequency limit, $kL \rightarrow 0$, maximum absorption will be obtained if we choose our parameters for a single liner system according to Eq. (14), which has been adapted for a cylinder with an anechoic end condition (σ being the porosity or open-area ratio of the sheet).

$$M_{h\,opt} = \frac{L\sigma}{2a} \tag{14}$$

However, such frequencies do not contribute significantly towards a dBA weighting. More specifically, the source noise is likely to be concentrated at considerably higher values. Maximizing broadband absorption as a general rule requires a high liner resistance. Eldredge derived an expression for peak resistance that we present here in a more relevant format.

$$M_{h\,opt} \approx (ka)\frac{r_h}{a}\left[\frac{4}{3\pi}\frac{t_h}{r_h} + \frac{1}{4}\left(\frac{t_h}{r_h}\right)^2\right]^{1/2} \tag{15}$$

This criterion is only a guideline and therefore not much use to a comprehensive optimization routine for anything other than the selection of starting values.

The optimization routine used here will be of a similar format to how conventional liners were treated in Section III. Using the Matlab tools, there are eight parameters that we wish to determine: cell depth, bias flow Mach number, aperture diameters, aperture pitches and liner thicknesses. The thickness of the perforated sheets is frequently assumed to be negligible and therefore insignificant yet Jing and Sun[12] have shown otherwise so we include it here. The problem is constrained in an appropriate way such that any solution does not breach the assumptions made and invalidate the model. We refer in particular to the assumptions of incompressible flow through the liner perforations and that the fluctuating field around each aperture can be treated in isolation.

The code has been modified to output attenuation levels for all the cut-on modes at the third-octave centre frequencies. If we allocate amplitudes for equal energy upstream in the same way as the conventional liners, it becomes possible to determine the amplitudes of the modes that will reach the end of the nozzle downstream and radiate to the atmosphere. As this model is an order of magnitude more advanced than the conventional liner one, the runtime has increased accordingly to the point where evaluating all the third-octave frequencies between 50Hz and 10kHz is no longer viable. As such, we will begin the optimization of blown liners by only considering frequencies up to 4kHz. A second optimization will also be run where we restrict out attention to a maximum of five radial modes cut-on for each of the first five azimuthal orders at all of the frequencies in an attempt to see how effective blown liners can be for these disturbances. Once either liner has been optimized, results for the full spectrum will be obtained to ensure that we are not masking another problem elsewhere. Finally, as cost function B has been shown to be a superior metric, we will use it exclusively from this point onwards.

C. Blown Liner Results

The results for the two optimization runs have been summarized below.

Table 3. Optimization results for blown liners.

Parameter		Optimization 1	Optimization 2
Cell depth, mm		470.2	500.0
Bias flow Mach number		0.05	0.05
Sheet A	Aperture radius, mm	1.40	1.00
	Aperture pitch, mm	5.61	4.00
	Sheet thickness, mm	0.50	0.50
Sheet B	Aperture radius, mm	1.34	5.00
	Aperture pitch, mm	10.88	100.0
	Sheet thickness, mm	0.50	10.0
Peak observer sound pressure level, dBA		84.70	85.21

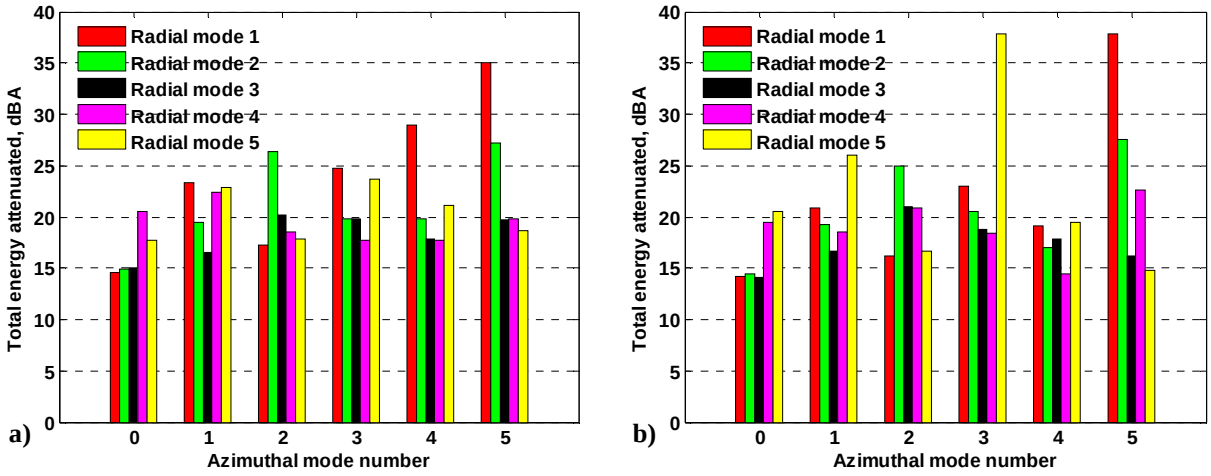

Figure 9. Integrated modal attenuation plots for the blown liners a) optimization 1, b) optimization 2.

In either case, the results may be considered somewhat disappointing. The overall levels of attenuation are substantially less than have been achieved for the conventional single and double layer liners. Further interrogation of the results reveals the reason for this to be the poor performance of the bias flow liners at higher frequencies. In contrast, at lower frequencies the situation is reversed. At 100Hz, the bias flow liner was capable of absorbing almost 20dB from the plane wave mode, whereas the double layer liner could barely remove a single decibel. This type of performance appears to come quite naturally to blown liners whereas to create any kind of effect on lower order modes at high frequencies, the geometry has to be pushed to extreme levels. Unfortunately, this behavior is consistent with that observed elsewhere. Howe[9] has shown theoretically that the effect on the fluctuating aperture flow is likely to be negligible for higher Strouhal numbers. This is primarily because the velocities induced by the vortex rings moving away from the perforated surface are more likely to cancel as the length scale of the vorticity is reduced. Initially, it was hoped that the good low frequency performance could be transferred to higher frequencies for low axial wavenumbers (i.e. higher order modes closer to cut-off) by increasing the blowing velocity to maintain a lower Strouhal number. The results show that blown liners can attenuate such modes reasonably well but not to the

same degree as a non-blown liner. Regrettably, lower frequencies are much less annoying to the observer and the bias flow liners fail to have much of an impact when the dBA weighting is applied.

D. Integration with Conventional Liners

The blown liners have not surpassed the performance of the conventional acoustic treatment based on a direct comparison. All that remains is to gain an estimate of whether there might be any benefits to be obtained by having a combination of the two models within the same nozzle. The authors recognize that the two models are not directly compatible due to the absence of the mean flow in the latter. However, we can obtain a crude first approximation by combining the attenuation directly between the two models and once more neglecting scattering effects at the interfaces. The extra modes cut-on by the action of the mean flow are heavily attenuated by the multi-specification liners. Therefore, if we consider inserting small amounts of blown liner, we can avoid having to evaluate the blown liner effects on these modes assuming that the attenuation of the other cut-on modes remains fairly similar. The results are summarized in Fig. 10 below.

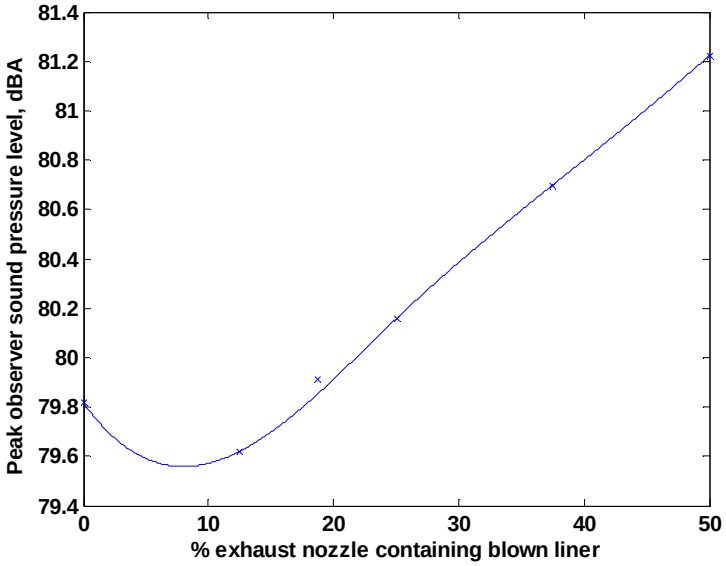

Figure 10. The variation in observer sound pressure level with increasing proportion of blown liner.

The data indicate that there may be a modest advantage in having a small segment of blown liner in the exhaust nozzle. This has arisen based on the system exploiting the excellent low frequency performance of the bias flow liner. The amount desired reflects the weighting given to these frequencies.

V. Conclusion

A number of simple liner models have been developed and numerically optimized for application to the Silent Aircraft exhaust nozzle design. The ultimate aim is to determine the most effective way of bringing fan rearward broadband noise in line with the Silent Aircraft noise goal. These include conventional liners (single layer, double layer, multiple segments) and blown liners. The estimates made for the blown liners involve the extension of an existing code, which currently lacks the presence of the mean flow. However, the results still provide an important insight into the abilities of this acoustic treatment for this application. An important part of the optimization process is the choice of an appropriate metric. Therefore, we have presented a comparison between two cost functions: the A-weighted residual acoustic power at the nozzle exit and the peak A-weighted sound pressure experienced by an observer on the ground. It was found that reductions in residual acoustic power do not always translate into a perceived benefit for the observer. For example, a reduction of 2dBA in peak observer sound pressure can be achieved whilst allowing the acoustic power to increase by 4dBA at the nozzle exit. For conventional acoustic treatments, we confirm that double layer liners can outperform single ones with the greatest benefits coming from multi-specification liners. Although, the optimized liner cell depths and sheet porosities are radically different

depending on the cost function chosen. Blown liners are effective at low frequencies so can complement conventional liners which work best at higher frequencies. However, A-weighting means that that for the Silent Aircraft design these low frequencies are relatively unimportant and the overall benefit of a blown liner segment appears to be small. The ongoing work with blown liners will involve the extension to mean flow in due course.

Appendix

A. Acoustic Power Evaluation in a Uniform Mean Flow

To evaluate the axial energy flux, we will use a generalized definition of acoustic intensity that accounts for the presence of a mean flow (see Morfey[6]). The overbars denote an average in time.

$$I_x = \overline{pu_x} + \frac{U_j}{\rho_j c_j^2}\overline{pp} + \frac{U_j^2}{c_j^2}\overline{pu_x} + \rho_j U_j \overline{u_x u_x} \tag{16}$$

The axial momentum equation provides a relationship between pressure and velocity.

$$-\frac{\partial p}{\partial x} = \rho_j \left[\frac{\partial u_x}{\partial t} + U_j \frac{\partial u_x}{\partial x} \right] \tag{17}$$

$$u_x = \frac{k_x p}{\rho_j \left(\omega - U_j k_x\right)} \tag{18}$$

We can define a non-dimensional modal admittance factor, η, as follows:

$$\eta = \rho_j c_j \frac{u_x}{p} = \frac{k_x a}{\left(ka - M_j k_x a\right)} \tag{19}$$

Eq. (16) can be rewritten in terms of normalized quantities and evaluated using Eq. (19).

$$I_x = \frac{|p|^2}{2\rho_j c_j}\left[\left(1 + M_j^2\right)\mathrm{Re}(\eta) + M_j\left(1 + |\eta|^2\right)\right] \tag{20}$$

The total sound power transmitted down the duct is obtained by integrating the intensity over the duct cross-section:

$$P = \int_S I_x dS = 2\pi \int_0^a I_x r dr \tag{21}$$

We can insert the expression for acoustic intensity in conjunction with a modal pressure term from Eq. (1).

$$P = \frac{\pi |A|^2}{\rho_j c_j}\left[\left(1 + M_j^2\right)\mathrm{Re}(\eta) + M_j\left(1 + |\eta|^2\right)\right] \int_0^a \left|J_n(k_r r)\right|^2 r dr \tag{22}$$

In general, the integral will have to be evaluated numerically. For the case of a rigid-walled duct, the radial wavenumbers and hence the values of the Bessel functions are purely real and we may take advantage of the following identity:

$$\int_0^a \left|J_n(k_r r)\right|^2 r dr = \int_0^a J_n^2(k_r r) r dr = \frac{a^2}{2}\left[J_n^2(k_r a) - J_{n-1}(k_r a) J_{n+1}(k_r a)\right] \qquad k_r \in \Re \tag{23}$$

Thus, the acoustic power for a single mode (n, m) in a rigid-walled duct may be simplified to:

$$P_{nm} = \frac{\pi a^2 \left|A_{nm}\right|^2}{2\rho_j c_j}\left[\left(1 + M_j^2\right)\eta_{nm} + M_j\left(1 + \eta_{nm}^2\right)\right]\left[J_n^2(k_r^{nm} a) - J_{n-1}(k_r^{nm} a) J_{n+1}(k_r^{nm} a)\right] \tag{24}$$

B. Multiple Liner Optimized Segment Details

This appendix contains the finer details of the different segments from the multiple liner optimization exercise using both cost functions.

Table 4. Multiple liner parameters optimized using cost function A.

Segment	1	2	3	4	5	6	7	8	9	10	11
Cell depth, mm	191.3	151.9	120.7	95.86	80.66	76.15	57.10	36.03	28.62	12.07	11.39
Sheet porosity, %	11.86	10.53	10.41	10.64	11.71	9.68	9.99	9.94	11.16	11.38	11.25
Length-to-diameter ratio	0.291	0.370	0.265	0.686	0.010	0.019	0.049	0.044	0.158	0.016	0.092

Table 5. Multiple liner parameters optimized using cost function B.

Segment	1	2	3	4	5	6	7	8	9	10	11	12	13
Cell depth, mm	202.6	191.3	151.9	120.7	90.50	48.05	38.16	32.11	25.51	20.26	12.78	9.59	9.05
Sheet porosity, %	6.67	6.36	6.10	6.00	9.11	6.58	6.81	6.30	6.03	6.00	7.08	6.49	6.68
Length-to-diameter ratio	0.150	0.059	0.208	0.066	0.021	0.293	0.292	0.215	0.100	0.025	0.018	0.524	0.029

Acknowledgments

The authors would like to thank the Cambridge-MIT Institute for funding this research. Prof. Jeff Eldredge is gratefully acknowledged for providing the fundamental routines for evaluating blown liner performance and for his guidance on their use. The authors are also indebted to Prof. Jeremy Astley and Dr. Gwénaël Gabard at ISVR for the use of their Matlab routines to evaluate the modal directivity patterns from a semi-infinite duct. Many other

members of the Silent Aircraft Initiative have made useful comments on liner optimization. In particular, special thanks must go to Dr. Anurag Agarwal for helpful discussions on the topics within this paper.

References

[1]Chapman, C. J., "Sound Radiation from a Cylindrical Duct. Part 1: Ray Structure of the Duct Modes and of the External Field," *Journal of Fluid Mechanics*, Vol. 281, No. 1, 1994, pp. 293-311.

[2]Keller, J., "Geometrical Theory of Diffraction," *Journal of the Optical Society of America*, Vol. 52, No. 2, 1961, pp. 116-130.

[3]Munt, R. M., "The Interaction of Sound with a Subsonic Jet Issuing from a Semi Infinite Cylindrical Pipe," *Journal of Fluid Mechanics*, Vol. 83, No. 4, 1977, pp. 609-640.

[4]Gabard, G. and Astley, R. J., "Theoretical Model for Sound Radiation from Annular Jet Pipes: Farfield and Nearfield Predictions," *Journal of Fluid Mechanics*, Vol. 549, No. 1, 2006, pp. 315-341.

[5]Eldredge, J. D. and Dowling, A. P., "The Absorption of Axial Acoustic Waves by a Perforated Liner with Bias Flow," *Journal of Fluid Mechanics*, Vol. 485, No. 1, 2003, pp. 307-335.

[6]Morfey, C. L., "Sound Transmission and Generation in Ducts with Flow," *Journal of Sound and Vibration*, Vol. 14, No. 1, 1971, pp. 37-55.

[7]Bechert, D. W., "Sound Absorption Caused by Vorticity Shedding, Demonstrated with a Jet Flow," *Journal of Sound and Vibration*, Vol. 70, No. 3, 1980, pp. 389-405.

[8]Howe, M. S., "The Dissipation of Sound at an Edge," *Journal of Sound and* Vibration, Vol. 70, No. 3, 1980, pp. 407-411.

[9]Howe, M. S., "On the Theory of Unsteady High Reynolds Number Flow through a Circular Aperture," *Proceedings of the Royal Society of London. Series A, Mathematical and Physical Sciences*, Vol. 366, 1979, pp. 205-223.

[10]Hughes, I. J. and Dowling, A. P., "The Absorption of Sound by Perforated Linings," *Journal of Fluid Mechanics*, Vol. 218, 1990, pp. 299-335.

[11]Zhao, H. and Sun, X., "Active Control of Wall Impedance," *AIAA Journal*, Vol. 37, 1999, pp. 825-831.

[12]Jing, X. and Sun, X., "Experimental Investigations of Perforated Liners with Bias Flow," *Journal of the Acoustical Society of America*, Vol. 106, No. 5, 1999, pp. 2436-2441.

[13]Eldredge, J. D., "On the Interaction of Higher Duct Modes with a Perforated Liner System with Bias Flow," *Journal of Fluid Mechanics*, Vol. 510, No. 1, 2004, pp. 303-331.

[14]Pierce, A. D., "Acoustics: An Introduction to Its Physic Principles and Applications," 2nd ed, The Acoustical Society of America, New York, 1989, pp. 104-106.

[15]Ko, S. H., "Sound Attenuation in Acoustically Lined Circular Ducts in the Presence of Uniform Flow and Shear Flow," *Journal of Sound and Vibration*, Vol. 22, No. 2, 1972, pp. 193-210.

[16]Guess, A. W., "Calculation of Perforated Plate Liner Parameters from Specified Acoustic Resistance and Reactance," *Journal of Sound and Vibration*, Vol. 40, No. 1, 1975, pp. 119-137.

[17]Motsinger, R. E. and Kraft, R. E., "Aeroacoustics of Flight Vehicles: Theory and Practice, Volume 2: Noise Control," edited by H. H. Hubbard, NASA RP-1258, 1991, pp. 165-206.

[18]Crichton, D., "Selection of Fan Design Parameters for SAX 20," CMI Silent Aircraft Initiative Report, Cambridge University Engineering Department, UK, Jan 2006.